Heliyon 5 (2019) e01628

Contents lists available at ScienceDirect

Heliyon

journal homepage: www.heliyon.com

Review Article

Characterization and densification of defect pyrochlore oxide powders $ABi_2Ta_5O_{16}$ (A=Na, Tl)

O. Ait Sidi Ahmed [a,*], L. Bourja [a], A. Chagraoui [a], A. Tairi [a], A. Moussaoui [a], H. Ait Oulahyane [a], B. Manoun [b], S. Villain [c]

[a] Laboratoire de Chimie Analytique et Physico-Chimie des Matériaux (LCAPM), Faculté des Sciences Ben M'Sik, Casablanca, Morocco
[b] Laboratoire des Sciences des Matériaux, des Milieux et de la modélisation (LS3M), Université Hassan 1er, 25000, Khouribga, Morocco
[c] Avenue de l'université Toulon Var B.P 20132, Laboratoire IM2NP, Bâtiment R83957, La garde CEDEX, Toulon, France

ARTICLE INFO

Keywords:
Inorganic chemistry
Materials chemistry

ABSTRACT

Defect pyrochlore oxide powders $ABi_2Ta_5O_{16}$, in the pseudo-binary systems $BiTaO_4$–ATa_3O_8 (A = Na, Tl), were prepared by solid state method. The structural study showed that all oxides crystallize in a cubic system with the space group *Fd3m*, the lattice parameter "a" were determined using Rietveld refinement method. For systematic study on densification from powders, the samples were pressed with a uniaxial pressure into pellets; sintering temperature, holding time and heating rate were optimized. Techniques, including X-ray diffraction, IR-Raman, MEB, dilatometry, were employed to investigate the structure and the morphology of the synthesized powders and sintered materials. The dielectric characteristics, relative permittivity and dielectric losses (tgδ), determined at room temperature are comparable to those of other pyrochlores.

1. Introduction

Among metallic oxides, compounds with general formula, $A_2B_2O_6O'$, where A and B are different cation species with different oxidation states (e.g. A^{3+} B^{4+} or A^{2+} B^{5+}) and O and O′ are anions, represent a family of phases isostructural to the mineral pyrochlore (NaCa) (NbTa)O6F/(OH). The pyrochlore structure possesses cubic symmetry with space group (*Fd3m*, Oh7), no. 227 and number of formula units (Z = 8). Four crystallographically nonequivalent kinds of atoms: A, B, O and O′ atoms occupy the 16d, 16c, 48f and 8b sites, respectively. The smaller B cations (16c) are six coordinated and located in a distorted octahedron formed by six oxygen ions O (48f). The larger A cations (16d) are eight-coordinated, located within a distorted cubic polyhedron formed by six O (48f) and 2 O' (8b). The structural formula is often written as B_2O_6•A_2O', which emphasizes that the arrangement consists of two interpenetrating networks of vertex-linked octahedra (B_2O_6) sharing corners, and a cuprite-like A_2O' tetrahedron [1]. This latter network is not essential for the stability of the structure and hence pyrochlore structure tolerates vacancies at A and O′ sites giving defect pyrochlore with formula $A_{2-x}\square_xB_2O_6O'_{1-y}\square'_y$ giving rise to different stoichiometries from AB_2O_6 to $A_2B_2O_6O'$. It is known that AB_2O_6 type defect pyrochlore are formed in the case where the A cation is a large monovalent metal such as Cs^+, Rb^+, Tl^+ or K^+ [2]. The site occupancy of the A cations in defect pyrochlore is insertion because the structural considerations reveal that in addition to the 16d and 8b sites there in another possible site (32e) depending on the size, charge and polarizability of the A cation either full or fractional occupation of any of the three sites is possible. Studies showed that the A ions in $RbTa_2O_5F$ occupy the 8b positions whereas in $TlNb_2O_5F$ the Tl cations are delocalized from the ideal 16d position to occupy the 32e positions statistically [2]. Pyrochlore mixed oxides have many technological applications thanks to theirs wide spectrum of properties (electrical, dielectric, magnetic, magneto-resistive, optical, electro-catalytic etc.) and can also be used as electrolytes or anode materials for solid electrolyte fuel cells (SOFC) and fixatives for radioactive waste due to theirs oxygen nonstoichiometry and to the distribution of cations in the structure [1]. Recently, Bi-based pyrochlores in the Bi_2O_3–ZnO–M_2O_5 (X = Sb, Ta and Nb) ternary systems have triggered great research interests owing to their relatively low sintering temperatures and excellent dielectric properties [3, 4, 5]. Some pyrochlore compounds occurring in the A_2O–Bi_2O_3- M_2O_5 system (A = Ag, Na, K, Tl and M = Nb, Ta) are attractive candidates for temperature-stable, low-loss, high-permittivity dielectric applications [6].

* Corresponding author.
E-mail address: oaitsidiahmed@gmail.com (O.A. Sidi Ahmed).

https://doi.org/10.1016/j.heliyon.2019.e01628
Received 18 February 2019; Received in revised form 30 April 2019; Accepted 30 April 2019

2. Experimental

The compounds $ABi_2Ta_5O_{16}$ (A = Na, Tl) were prepared by usual solid state reaction from starting reagents Bi_2O_3 (Sigma-Aldrich, 99.9%), Ta_2O_5 (Sigma-Aldrich, 99%) Na_2CO_3 and Tl_2CO_3 (Sigma-Aldrich, 99.9%) Weighted quantities of the reactants were intimately mixed and ground in an agate mortar. In order to avoid a possible oxidization of Tl^+ to Tl^{3+}, all compounds were treated under nitrogen atmosphere. Three thermal processings with intermittent regrinding at 300 °C (6 hours) (to provoke the departure of CO_2 and in the same time to avoid volatilization of Tl_2CO_3 [7], 800 °C (12 hours) and 950–1000 °C (12 hours) were necessary to obtain the final compounds. X-ray powder diffractograms were obtained using Cu Kα line of a D5000 Siemens diffractometer equipped with a back monochromator. The data were recorded between 10 and 120 (2θ) in steps of 0.04° with a count time of 72 s. Temperature programmed X-ray diffraction was performed on a Siemens D5000 diffractometer fitted out with an ANTON PARR furnace (CHTK10) and a linear detector (Elphyse 14°). The powder of each prepared compound was ground and mixed with 5% of polyvinyl alcohol and polyethylene glycol and pressed using a uniaxial pressure 200 MPa into pellets with a diameter of 10 mm and thickness of about 2 mm. The sintering behavior of the powders was investigated by dilatometric method. The powders were uniaxially pressed at 200 MPa and the compacts were sintered in the vertical dilatometer (SETARAM TMA92) up to 1400 °C under air sweeping with heating rates of 3 °C/min. The relative densities were also calculated from comparisons of densities which are determined geometrically and theoretically. The surface morphologies of the samples were examined by scanning electron microscopy (SEM). The IR spectra were recorded in the range of 400–4000 cm^{-1} with 4 cm^{-1} resolution using a Fourier-Transformed BOMEN MX spectrometer from dicks containing 2% of the sample and 98% of KBr or CsCl. Infrared active phonon modes are attributed to the vibrations of ions in the crystal lattice. Raman measurements were done in a DILOL-XY type Raman spectrometer equipped with a triple monochromator in order to examine lattice vibration and hence local structure of materials. All spectra were obtained at room temperature. The excitation source is an argan-ion laser (5W) and the emission line used is 514.5 nm (Spectra Physics, 20 mW). Before sintering, the pellets were heated at 500 °C to evaporate the binder. After being electrode with post-fired silver paste on two major surfaces of the disk pellets, dielectric properties were measured at room temperature as a function of the frequency (1000 Hz - 10MHz) by using a HP 4194A bridge of impedance analyzer.

3. Results and discussion

3.1. Structural analyses

3.1.1. XRD diffraction

The phase structures of the $ABi_2Ta_5O_{16}$ (A = Na, Tl) samples were determined by XRD patterns, as shown in Fig. 1. All characteristic peaks belong to a cubic pyrochlore and are fully indexed based on space group, *Fd3m* [8]. No impurity phases were detected in the XRD pattern of the three compounds $NaBi_2Ta_5O_{16}$ and $TlBi_2Ta_5O_{16}$ indicating that the sample was phase-pure pyrochlore. These results are shown in Table 1. The lattice parameter of the $ABi_2Ta_5O_{16}$ (A = Na, Tl) compounds determined from the Rietveld refined XRD pattern are $a = 10.5013$ (1) Å and 10.5144 (1) Å, respectively, for $NaBi_2Ta_5O_{16}$ and $TlBi_2Ta_5O_{16}$.

3.1.2. Infrared spectroscopy

The group theoretical analysis of the normal vibration of the ideal pyrochlore structure predicts 26 normal modes [9]: $A_{1g}+E_g+2F_{2g}+4F_{1u}+3A_{2u}+3E_u+8F_{1u}+4F_{2u}$. Only A_{1g}, E_g, $4F_{2g}$ and $8F_{1u}$ (one of eight F_{1u} modes refers to acoustic vibrations) are Raman active and infrared active respectively. The IR spectra for $NaBi_2Ta_5O_{16}$ and $TlBi_2Ta_5O_{16}$, are represented in Fig. 2 We note at first that these spectra are similar to those of others pyrochlores prepared in [10].

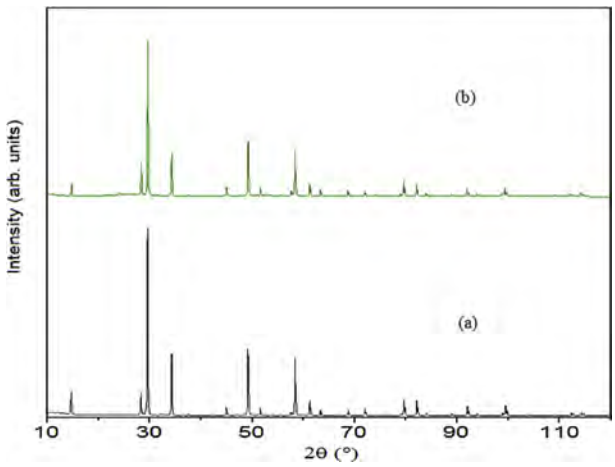

Fig. 1. XRD patterns of $NaBi_2Ta_5O_{16}$ (a) and $TlBi_2Ta_5O_{16}$ (b).

Table 1
X-ray powder data observed (obs.) and calculated (calc.) for $NaBi_2Ta_5O_{16}$ and $TlBi_2Ta_5O_{16}$.

	$NaBi_2Ta_5O_{16}$			$TlBi_2Ta_5O_{16}$		
hkl	$d_{obs.}$ (Å)	$d_{calc.}$ (Å)	I (%)	$d_{obs.}$ (Å)	$d_{calc.}$ (Å)	I (%)
111	6.06	6.06	16	6.07	6.07	9
220	3.713	3.712	<1	3.718	3.717	1
311	3.166	3.166	11	3.170	3.170	21
222	3.0315	3.0314	100	3.0353	3.0352	100
400	2.6253	2.6253	35	2.6286	2.6286	29
331	2.4092	2.4091	1	2.4122	2.4121	1
422	2.1435	2.1436	<1	2.1463	2.1462	<1
511	2.0209	2.0210	2	2.0235	2.0235	3
440	1.8563	1.8564	41	1.8587	1.8587	38
531	1.7750	1.7750	4	1.7773	1.7772	6
442	-	1.7502	-	1.7524	1.7524	<1
620	1.6604	1.6604	<1	1.6625	1.6624	<1
533	1.6014	1.6014	1	1.6034	1.6034	4
622	1.5831	1.5831	36	1.5851	1.5851	33
444	1.5157	1.5157	10	1.5176	1.5176	9
551	1.4704	1.4705	2	1.4723	1.4723	3
731	1.3671	1.3671	3	1.3689	1.3688	4
800	1.3127	1.3127	5	1.3143	1.3143	4
733	1.2829	1.2829	<1	1.2845	1.2845	1
644	-	1.2735	-	1.2751	1.2751	<1

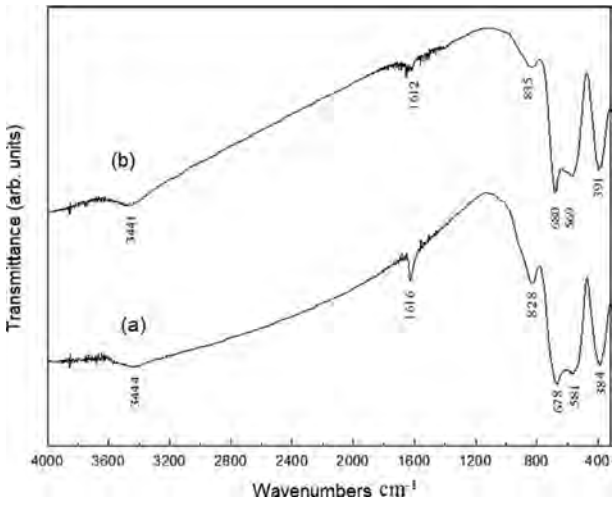

Fig. 2. Infrared transmission spectra of $NaBi_2Ta_5O_{16}$ (a) and $TlBi_2Ta_5O_{16}$ (b).

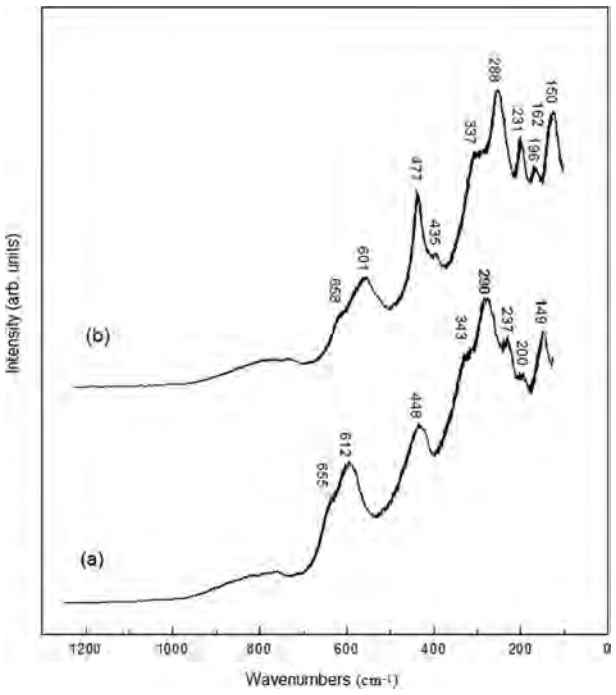

Fig. 3. Raman spectra of $NaBi_2Ta_5O_{16}$ (a) and $TlBi_2Ta_5O_{16}$ (b).

The Infrared vibrational frequencies observed at around 840 and 490 cm^{-1} attributed to the Bi–O′ stretching can be assigned on the one hand to the shorter bond distance (2.20 Å) and on the other hand to longer (2.40 Å) bond distance Bi–O' [11]. The static disorder of Bi and O' is associated with tendency of lone pair electron of Bi ($6s^2$) to be stereo-chemically active [11]. The band in the region 560–700 cm^{-1} can be ascribed to Ta–O stretching vibration. These later are usually broadened with shoulder probably due to distortions in the TaO_6 octahedra as for $Cd_2Ta_2O_7$ [12]. The vibrational modes at about 390–400 cm^{-1} have been assigned to fundamental Bi–O stretching. The absorption bond at 3500 cm^{-1} is related to O–H stretching vibrations, whereas the bond near to 1630 cm^{-1} represents H···O···H bonding vibration of water.

3.1.3. Raman diffusion

Based on the group theoretical analysis the ideal pyrochlore structure has 26 normal vibrating modes, among these 26 modes only A_{1g}, E_g, $4F_{2g}$ modes are Raman-active (R). From the Raman spectra which presented Fig. 3(a) and (b), the Raman peaks are observed at 149, 200, 237, 290, 343, 448, 612 and 655 cm^{-1} for $NaBi_2Ta_5O_{16}$ and at 150, 196, 231, 288, 237, 435, 477, 601 and 658 cm^{-1} for $TlBi_2Ta_5O_{16}$. These observed Raman peaks can be assigned to symmetry species by referencing the previous literatures on diverse pyrochlore oxides [13, 14, 15, 16]. It is noticed that more than six Raman bands (predicted for the ideal pyrochlore structures) are observed, which implies the existence of some additional displacements of the A and O′ sites in the bismuth pyrochlore structure [14]. The sharp peak with lower frequency (150 cm^{-1}) is assigned to a O′-Bi-O′ bending vibration and corresponds to F_{1u} mode. Similar mode is observed in the Raman spectra of other cubic bismuth pyrochlores such as $Bi_{1.5}Zn_{0.92}Nb_{1.5}O_{6.92}$, $Bi_{1.5}ZnTa_{1.5}O_7$, and $Bi_{1.5}MgTa_{1.5}O_7$ [14].

The ideal $A_2B_2O_7$ (or $A_2B_2O_6O'$) cubic pyrochlore can be described as two interpenetrating networks A_2O' (network of A_4O' tetrahedra as seen in anticristobalite Cu_2O type structure) and B_2O_6 (3D-network of corner shared BO_6 octahedra). The variations occurred in A atoms environment and in A-O′ bond length can be the consequence of A and O′ atoms displacement from their ideal positions in the $O'A_2$ network. The observed peak at about 237 cm^{-1} is attributed to F_{2g} mode, corresponding to the stretching vibration of O–B–O bond. The frequency at around of 343 cm^{-1} is assigned to the stretching vibration of A-O bond, which is assigned to the (E_g and F_{2g}) mode. The A_{1g} mode observed at 477 cm^{-1} is attributed to the stretching vibration of the B–O bond in BO_6 octahedra. For many pyrochlores, the F_{2g} mode is observed at high frequency band around 600 cm^{-1}, for examples, at 598 cm^{-1} for $Er_2Mn_2O_7$ [17], at 590 cm^{-1} for $Yb_2Ti_2O_7$ [13], and at 590 cm^{-1} for $La_2Zr_2O_7$ [18]. In this work, the frequency band assigned to F_{2g} mode is observed in the range 601–612 cm^{-1}, while the A_{1g} mode at 655 cm^{-1} corresponds to the breathing mode of the O octahedra [19, 20]. All the observed Raman modes can be attributed to the relaxation of the selection rules and they show a reduction in symmetry of these samples due to the displacement of the bismuth ions in Bi-based pyrochlore.

3.2. Densification

3.2.1. Raw powder

The morphology of the raw powder of $NaBi_2Ta_5O_{16}$ and $TlBi_2Ta_5O_{16}$ obtained by solid state reaction is illustrated in Fig. 4 (a) and (b). It consists of grain sizes of around 1μm. we note also in the raw powder the presence of agglomerates, large grains surrounded by smaller ones. This phenomenon seems to be related to a pre-sintering generated by the method of preparation.

3.2.2. Binder influence

Different samples from the powder have been cold-pressed without adding organic binder did not make good pellets of good mechanical strength. In order to improve the raw quality of the pellets, an addition of binder consisting of a mixture of ultrapure water, polyvinyl alcohol (PVA 4/125) and polyethylene glycol (PEG 1500) has been added to the powder.

3.2.3. Pressure influence

Various powder samples of $NaBi_2NbTa_5O_{16}$ and $TlBi_2Ta_5O_{16}$ compounds were pressed into pellets between 50 and 400 MPa giving density

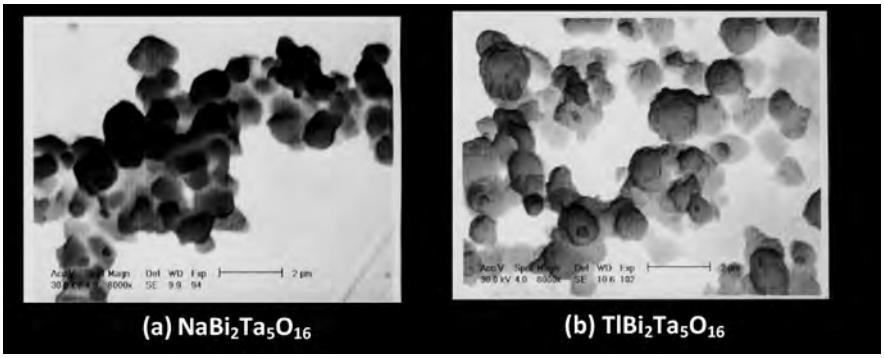

Fig. 4. SEM images powders of $NaBi_2Ta_5O_{16}$ (a) and $TlBi_2Ta_5O_{16}$ (b).

before sintering between 60% and 70%. By using the same thermal cycle, pellets were sintered and give density between 70% and 92%. Fig. 5 (a) and (b) shows the typical evolution of density versus pressure before and after sintering (a) for $NaBi_2NbTa_5O_{16}$ and (b) for $TlBi_2NbTa_5O_{16}$. We can notice that on the one hand the density in raw pellets increases regularly with pressure and on the other hand the density of the sintered materials showed the highest density located around 200 MPa. Density of sintered materials did not increase any further at higher pressing, above 200 MPa. This latter was retained as optimal pressure, so all powders were uniaxially pressed at 200 MPa.

3.2.4. Elimination of binder

Before sintering, it is necessary to begin with the first step of elimination of binder. According to commercial data on the thermal characteristics of PVA and PEG, we started the sintering process at 500 °C with low heating rate to burn organic matter without cracking pellets [21, 22]. For this reason, the choice of the heating rate is set at 5 °C/min with holding at 500 °C for 1 hour to ensure complete elimination of binder.

The density percentage D (%) after sintering was carried out using the following formula:

$$D = \frac{\rho_{exp}}{\rho_{th}}$$

The theoretical density (ρ_{th}) was calculated from the diffraction patterns applying the formula:

$$\rho_{th} = \frac{Z \times M}{N \times V}$$

Where:

- M: Molar mass of sample
- Z: Number of formula units
- N: Avogadro number
- V: Volume of the cell

The experimental density (ρ_{Exp}) was determined from diameter and thickness of pellets applying the formula:

$$\rho_{exp} = \frac{m_p}{\pi \times \left(\frac{\varnothing}{2}\right)^2 \times e}$$

Where:

- m_p: Mass of pellet
- ϕ: Diameter of pellet
- e: Thickness of pellet

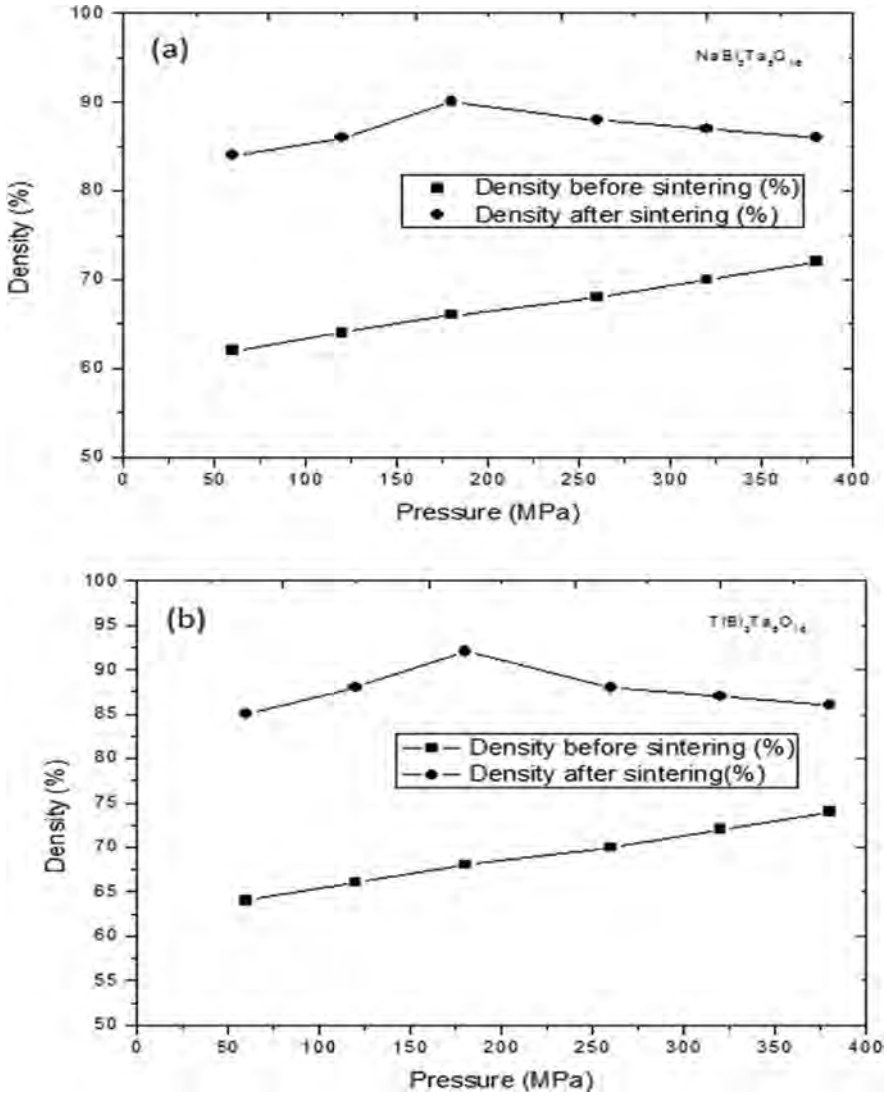

Fig. 5. Pressure versus density before and after sintering for $NaBi_2NbTa_5O_{16}$ (a) and $TlBi_2Ta_5O_{16}$ (b).

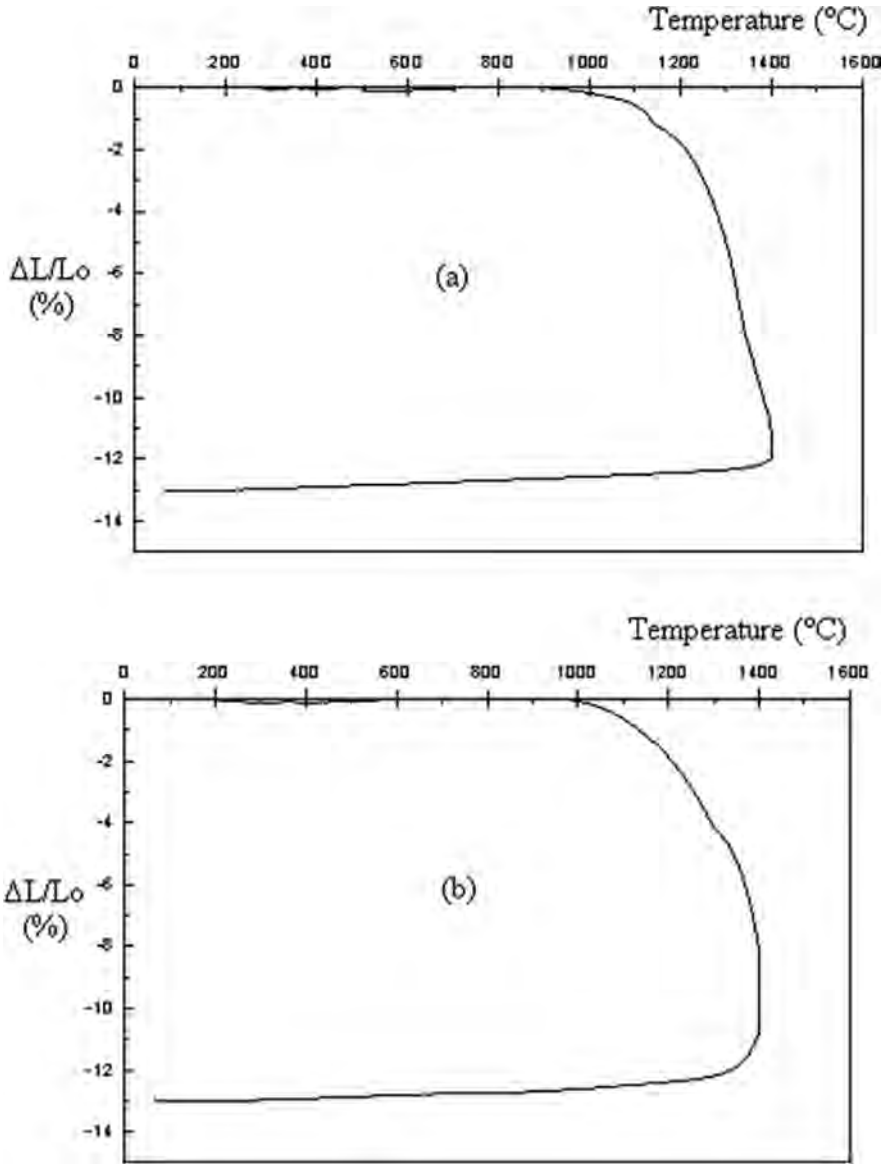

Fig. 6. Dilatometry curves of $NaBi_2NbTa_5O_{16}$ (a) and $TlBi_2Ta_5O_{16}$ (b).

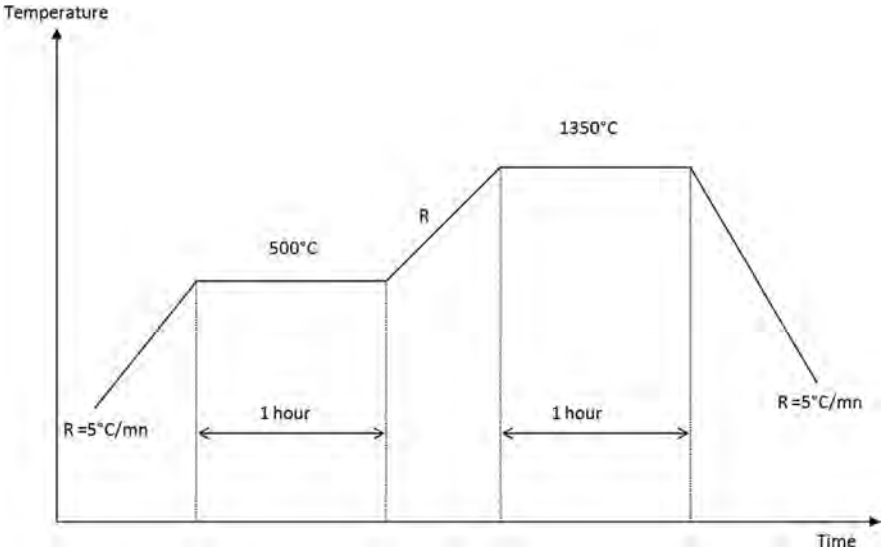

Fig. 7. Sintering thermal cycle.

Table 2
Characteristics of the thermal sintering adopted for $ABi_2MTa_5O_{16}$ (A = Na, Tl) compounds.

Compounds	Temperature (°C)	Holding time (h)	Densification (%)
$NaBi_2Ta_5O_{16}$	1330	1	90
$TlBi_2Ta_5O_{16}$	1380	1	92

3.2.5. *Sintering temperature influence*

After using heating rate at (5 °C/min), different attempt to determine sintering temperatures were applied to the pellets corresponding to $NaBi_2Ta_5O_{16}$ and $TlBi_2Ta_5O_{16}$. We note that between 1000 and 1400 °C, the density rises with temperatures and passes for both samples from 70% to 90% for $NaBi_2Ta_5O_{16}$ and from 73% to 92% for $TlBi_2Ta_5O_{16}$ but in parallel with this increase in density; we noted a slight loss of mass

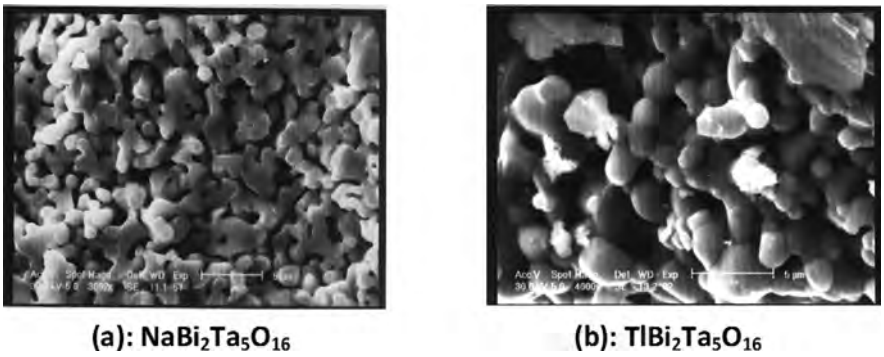

Fig. 8. SEM images of $NaBi_2NbTa_5O_{16}$ (a) and $TlBi_2Ta_5O_{16}$ (b) sintered at about 1350 °C.

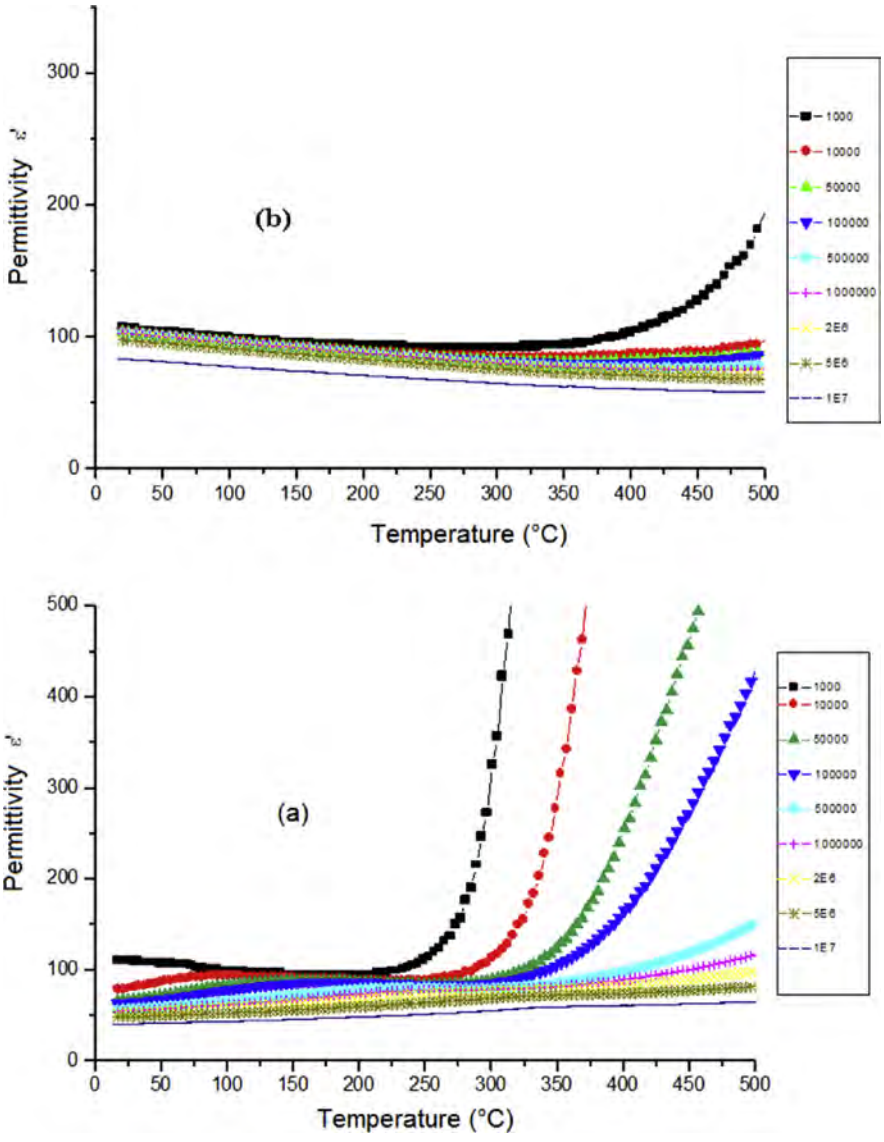

Fig. 9. Frequency dependence of dielectric constant vs. temperature of $NaBi_2Ta_5O_{16}$ (a) and $TlBi_2Ta_5O_{16}$ (b).

observed and became significant at 1400 °C. So, we have to find exactly optimal sintering temperatures. We have used dilatometry curves which consist to measure the evolution of ΔL/Lo as a function of temperature Fig. 6 (a) and (b).

Analysis of these curves leads to distinguish two regions:

- The first region, between room temperature and 1000 °C, characterized by a weak variation of ΔL/Lo (no shrinkage).
- The second region, between 1000 and 1400 °C for the two compounds indicate notable variations of ΔL/Lo characterized by the beginning and ending of shrinkage process.

During the sintering process we have found that at optimal sintering temperature, sintering reaches its maximum. Treatments carried above 1400 °C do not affect density but only contribute to increase mass losses of pellets. So, the optimal sintering temperature chosen for both pressed samples to increase densification and to decrease losses of mass, was 1330 °C and 1380 °C respectively for $NaBi_2Ta_5O_{16}$ and $TlBi_2Ta_5O_{16}$.

3.2.6. *Influence of the holding time*

The effects of holding time (HT) between 1330 and 1380 °C for both compounds was investigated and for one hour at optimal temperatures leads to a reasonable densification (90–92%). Longer heating times do not improve the density, but promote the sublimation of the material elements.

3.2.7. *Thermal cycle*

Given the influence of the parameters studied above sintering heating, heating rate and heating time, we performed the thermal cycle shown in Fig. 7.

A first step for one hour at 500 °C allowing the total elimination of the binder used and a second step also for one hour at sintering temperature to reach good density of pellets. The characteristics of the thermal sintering cycles used are summarized in Table 2.

The morphological examination under the scanning electron microscope (SEM) of the sintered pellets, reveals the presence of relatively large grains (~5 μm) showing angles of 60–120°, indicating a good densification of the materials (Fig. 8 (a) and (b)).

3.3. *Dielectric properties*

Fig. 9 and Fig. 10 show frequency and temperature dependence of dielectric properties (dielectric constant and dielectric loss tanδ) for

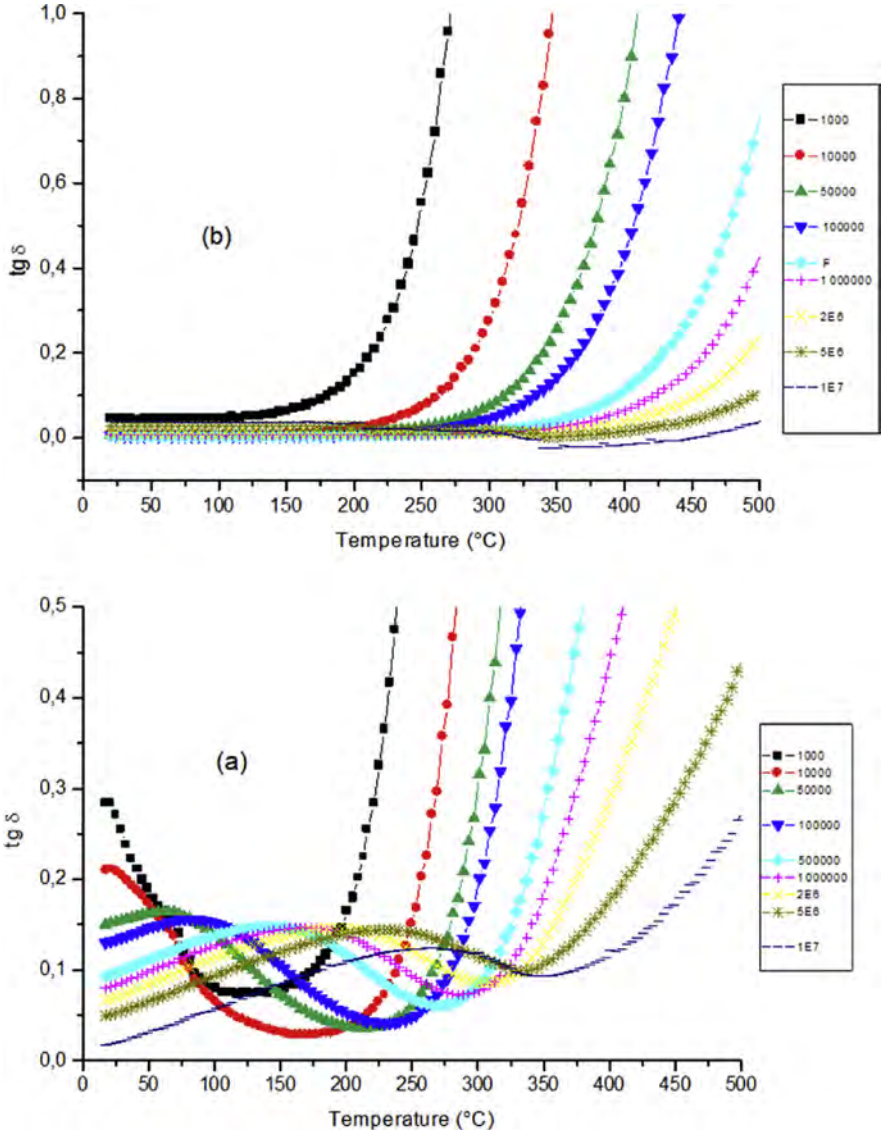

Fig. 10. Frequency dependence of dielectric losses vs. temperature of $NaBi_2Ta_5O_{16}$ (a) and $TlBi_2Ta_5O_{16}$ (b).

Table 3
Dielectrics characteristics of $ABi_2MTa_5O_{16}$ (A = Na, Tl) compared with others in the literature.

Compound	Relative density (%)	ε	tgδ	$\tau_\varepsilon = \Delta\varepsilon/\varepsilon\Delta T.10^6$ (K^{-1}) (ppm/°C)	Reference
$Bi_{1.5}Nb_{1.5}Zn_{0.92}O_{6.92}$	94	178	-	−647	[23]
$Bi_{3.5}Mg_{1.8}Ta_{2.7}O_{13.8}$	-	84	0.001	−328	[9]
$RbBi_2Ta_5O_{16}$	-	70	0.266	-	[24]
$NaBi_2Ta_5O_{16}$	90	110	0.284	−1327	(This work)
$TlBi_2Ta_5O_{16}$	92	107	0.045	−953	(This work)

Table 4
Frequency and temperature corresponding to the maximum of tgδ for $NaBi_2Ta_5O_{16}$.

$F_{max.}$(Hz).10^{-4}	1	5	10	50	100	200	500	1000
$T_{max.}$ (K)	294	338	358	414	442	470	506	546

$NaBi_2Ta_5O_{16}$ (a) and for $TlBi_2Ta_5O_{16}$ (b) compounds. The examination of these curves shows that the dielectric constants at low frequencies from 1 kHz to 10 MHz exhibit a frequency independent characteristic and dielectric constants values are in the range of 107–110. Table 3 shows the dielectric constant temperature coefficients.

3.3.1. Raw powder

We have mentioned in an earlier work [8] that the plots of dielectric loss for $NaBi_2Ta_5O_{16}$ exhibit maximum of tanδ which shifted towards higher temperature when frequency increases, in this paper we continue the explication of this phenomenon.

3.3.2. Temperature dependence of dipolar polarization in $NaBi_2Ta_5O_{16}$

The analysis of the dielectric losses (tgδ) of the compound $NaBi_2Ta_5O_{16}$ presented in Fig. 10 shows the presence of a maximum which varies with temperature and with frequency. The maximum tgδ value shifts, due to increasing temperature from, to lower values. This phenomenon is related to dielectric relaxations and is considered as intrinsic property for some materials [26, 27].

In Table 4 we have reported values of temperatures T_{max} and of frequencies F_{max} corresponding to the maximum tgδ for the compound $NaBi_2Ta_5O_{16}$. This phenomenon varies with reciprocal of measuring temperature obeying Arrhenius relation, given by: $F_{max}{}^{\circ} = {}^{\circ}F_oExp\ (-Ea/KT_{max})$. The slope of the log ($F_{max}$) vs. f ($1/T_{max}$) ($K^{-1}$) plot in Fig. 11 will be equal to (-Ea/k) as given in Arrhenius relation. Relaxation activation energies were determined due to experimental measurement of the dielectric loss peaks as a function of temperature.

From this plot we can calculate the activation energy corresponding to the relaxation phenomenon: Ea = (0.16 ± 0.01) eV.

There are several other important parameters which can be also obtained from dielectric data. τ_o, relaxation time can be calculated from the data such as shown in figure 13. Values of 10^{-12} to 10^{-14}s are indicative that the relaxation process is ionic in origin. However, very low values of τ_o are suggestive that the relaxation process is electronic space charge polarization [25, 26, 27]. In our case, $\tau_o = 0.6\ 10^{-13}$ s ($\tau_o = 10^{-12}$ s for the pyrochlore phase $Pb_{1,83}Nb_{1,72}Mg_{0,29}O_{6,39}$).

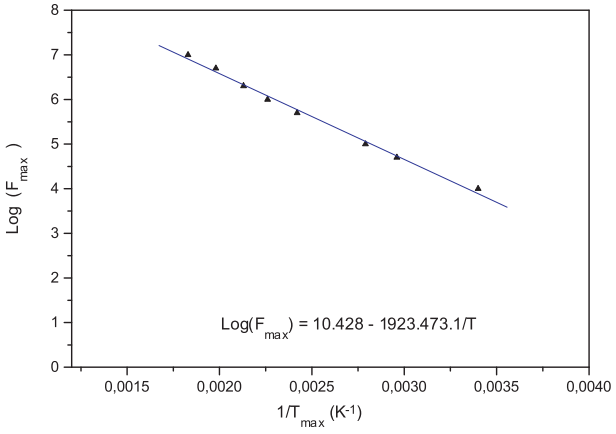

Fig. 11. Frequency Logarithmic temperature dependence of the frequency location at the dielectric losses peak for compound $NaBi_2Ta_5O_{16}$ heated from 25 °C to 500 °C.

4. Conclusions

Defect pyrochlore oxide powders $NaBi_2Ta_5O_{16}$ (A = Na, Tl) have been prepared by the solid state method and characterized by powder XRD and infrared and Raman spectroscopies. Both materials crystallize in the cubic crystal lattice with *Fd3m* space group. The infrared and Raman bands observed for these compositions are consistent with the Raman spectra expected for defect pyrochlores, $ABB'O_{7-x}$. The morphology of sintering ceramics indicates a good densification of the materials. The dielectric constants of the samples are in the range of 107–110 together with a negative temperature coefficient of permittivity. Dielectric losses (tgδ) of the compound $NaBi_2Ta_5O_{16}$ presented maximum versus temperature and frequency, this phenomenon is related to dielectric relaxations. The activation energy Ea and relaxation time τ_o corresponding to this phenomenon were found to be 0.16 eV and $0.6\ 10^{-13}$ s, respectively. Such dielectric and electrical properties make the compound $NaBi_2Ta_5O_{16}$ attractive in the applications of ceramic capacitor and resonators.

Declarations

Author contribution statement

Omar Ait Sidi Ahmed: Conceived and designed the experiments; Analyzed and interpreted the data; Wrote the paper.

Abdeslam Chagraoui, Abdennajib Moussaoui, Sylvie Villain, Abdelmjid Tairi, Lamia Bourja, Hajar Ait Oulahyane: Analyzed and interpreted the data.

Bouchaib Manoun: Analyzed and interpreted the data; Contributed reagents, materials, analysis tools or data.

Funding statement

This research did not receive any specific grant from funding agencies in the public, commercial, or not-for-profit sectors.

Competing interest statement

The authors declare no conflict of interest.

Additional information

No additional information is available for this paper.

References

[1] M.A. Subramanian, G. Aravamudan, G.V. SubbaRao, Oxide pyrochlores -A review, Prog. Solid State Chem. 15 (1983) 55–143.
[2] S. Yonezawa, Y. Muraoka, Y. Matsushita, Hiroi, Superconductivity in a pyrochlore-related oxide KOs_2O_6, J. Phys. Condens. Matter 16 (2004) 9–12.
[3] K. Sudheendran, K.C.J. Raju, M.V. Jacob, Microwave Dielectric Properties of Ti-Substituted $Bi_2(Zn_{2/3}Nb_{4/3})O_7$ Pyrochlores at Cryogenic Temperatures, J. Am. Ceram. Soc. 92 (6) (2009) 1268–1271.
[4] H.J. Youn, T. Sogabe, C.A. Randall, T.R. Shrout, M. T, Phase Relations and Dielectric Properties in the Bi_2O_3–ZnO–Ta_2O_5 System, J. Am. Ceram. Soc. 84 (2001) 2557–2562.
[5] C.C. Khaw, K.B. Tan, C.K. Lee, High temperature dielectric properties of cubic bismuth zinc tantalate, Ceram. Int. 35 (2009) 1473–1480.

[6] O. Ait Sidi Ahmed, A. Tairi, A. Chagraoui, S. Khairoun, J.C. Champamaud, B. Frit, Nouveaux matériaux $ABi_2B_5O_{16}$(A=Na,Ag,K,Rb,Tl et B=Nb,Ta) de type purochlore déficitaire, Ann. Chim. Sci. Mat. 25 (2000) 201–209.

[7] M. Bouchama, M. Tournoux, Revue de Chimie Minérale, t12, 1969, p. 80.

[8] O. Ait Sidi Ahmed, A. Tairi, A. Chagraoui, S. Khairoun, J.C. Champamaud, B. Frit, Dielectric properties of new defect pyrochlore compounds $AB_2M_5O_{16}$ (A=Na,K,Tl FOR M=Ta, andA=K,Tl FROM M=Nb), Ann. Chim. Sci. Mat. 25 (suppl. 1) (2000) 181–186.

[9] P.Y. Tan, K.B. Tan, C.C. Khaw, Z. Zainal, S.K. Chen, M.P. Chon, Structural and electrical properties of bismuth magnesium tantalate pyrochlores, Ceram. Int. 38 (2012) 5401–5409.

[10] M. Chen, D.B. Tanner, J.C. Nino, Infrared study of the phonon modes in bismuth pyrochlores, Phys. Rev. B 72 (2005) 054303.

[11] M.T. Vendenborre, E. Husson, Comparison of the force field in various pyrochlore families. I. The $A_2B_2O_7$ oxides, J. Solid State Chem. 50 (1983) 362.

[12] H.C. Gupta, S. Brown, N. Rani, V.B. Gohel, Lattice dynamic investigation of the zone center wavenumbers of the cubic $A_2Ti_2O_7$ pyrochlores, J. Raman Spectrosc. 32 (2001) 41–44.

[13] A. Garbout, S. Bouattour, A.W. Kolsi, Sol–gel synthesis, structure characterization and Raman spectroscopy of $Gd_{2-2x}Bi_{2x}Ti_2O_7$ solid solutions, J. Alloy. Comp. 469 (2009) 229–236.

[14] L.B. Gao, S.W. Jiang, R.G. Li, B. Li, Y.R. Li, Structure and dielectric properties of rf sputtered Bi_2O_3–MgO–Nb_2O_5 pyrochlore thin films, Ceram. Int. 40 (2014) 4225–4229.

[15] W. Xia, et al., Dielectric properties and atomic-scale microstructural characterizations of cubic-pyrochlored ceramics in the system of Bi_2O_3-MgO-Nb_2O_5, J. Alloy. Comp. 701 (2017) 682–688.

[16] Yangyang Li, Xinhua Zhu, T.A. Kassab, Atomic-scale microstructures, Raman spectra and dielectric properties of cubic pyrochlore-typed $Bi_{1.5}MgNb_{1.5}O_7$ dielectric ceramics, Ceramics Int. 40 (6) (2014) 8125–8134.

[17] S. Brown, H.C. Gupta, J.A. Alonso, M.J. Martinez-Lope, Vibrational spectra and force field calculation of $A_2Mn_2O_7$ (A =Y, Dy, Er, Yb) pyrochlores, J. Raman Spectrosc. 34 (2003) 240–243.

[18] M.T. Vanderborre, E. Husson, H. Brusset, Analyse en coordonnées normales des composés $A_2^{III}B_2^{IV}O_7$ (A = La, Nd; B = Zr, Hf) de structure pyrochlore, Spectrochim. Acta Part A 37 (1980) 113–118.

[19] S. Kamba, H. Hughes, D. Noujni, S. Surendran, R.C. Pullar, P. Samoukhina, J. Petzelt, R. Freer, N.M. Alford, D.M. Iddles, Relationship between microwave and lattice vibration properties in $Ba(Zn_{1/3}Nb_{2/3})O_3$-based microwave dielectric ceramics, J. Phys. D Appl. Phys. 37 (2004) 1980–1986.

[20] F. Shi, H. Dong, Correlation of crystal structure, dielectric properties and lattice vibration spectra of $(Ba_{1-x}Sr_x)(Zn_{1/3}Nb_{2/3})O_3$ solid solutions, Dalton Trans. 40 (2011) 6659–6667.

[21] D. Bernache-Assollant, Chimie Physique de Frittage FORCERAM, Editions Hermèses Paris, 1993.

[22] R.A. Dimilia, J.S. Reed, Dependence of compaction on the glass transition temperature of the binder phase, Am. Ceram. Soc. Bull. 62 (4) (1983) 484.

[23] A.F. Qasrawi, Bayan H. Kmail, A. Mergen, Synthesis and characterization of Bi1.5Zn0.92Nb1.5−xSnxO6.92−x/2 pyrochlore ceramics, Ceram. Int. 38 (2012) 4181–4187.

[24] M.K. Ehlert, J.E. Greedan, M.A. Subramanian, Novel defect pyrochlores $ABi_2B_5O_{16}$ (A = Cs, Rb; B = Ta, Nb), J. Solid State Chem. 75 (1988) 188.

[25] B. Dominique, Thèse, Université de Rennes, 1976.

[26] L.L. Hench, J.K. West, Principes of Electronic Ceramic, Wily-Interscience, 1988, p. 205.

[27] T.R. Shrout, S.L. Swartz, Dielectric properties of pyrochlore lead magnesium niobate, Mater. Res. Bull. 18 (1983) 663.